Journal of Hydrology 620 (2023) 129392

Contents lists available at ScienceDirect

Journal of Hydrology

journal homepage: www.elsevier.com/locate/jhydrol

Research papers

Towards a better understanding of flow-related processes in the vertically distributed compartments of karst aquifers by combining natural tracers and stable isotopes

B. de la Torre *, J.M. Gil-Márquez, M. Mudarra, B. Andreo

Department of Geology and Center of Hydrogeology at the University of Malaga, Faculty of Science, Malaga E-29071, Spain

ARTICLE INFO

This manuscript was handled by C. Corradini, Editor-in-Chief, with the assistance of Frédéric Huneau, Associate Editor

Keywords:
Natural soil tracers
Unsaturated zone
Stable isotopes
Karst aquifer
south Spain

ABSTRACT

Understanding infiltration pathways throughout the different compartments of karst systems (soil-epikarst-unsaturated zone-saturated zone) is vital to assess recharge processes, vulnerability to pollution, and the general hydrogeological functioning of these kind of aquifers. To gain deeper insight into the soil-water-rock hydrogeochemical processes occurring throughout the vertically hierarchized compartments of the aquifer and to evaluate the applicability of different soil natural parameters as groundwater flow tracers, the present work analyzes the spatial and temporal evolution of total organic carbon -TOC-, intrinsic fluorescence related to organic matter, nitrates, $\delta^{13}C_{TDIC}$, and the values of stable isotopes of $\delta^{2}H$ and $\delta^{18}O$ from water molecules and at different sampling points in a geologically complex karst aquifer in south Spain (Jarastepar carbonate massif). Over two years, rain and soil water (30 and 60 cm deep) samples were collected simultaneously at an experimental plot along with groundwater from the top of the saturated zone and a base-level spring. Results show that the variation in the concentration of natural soil tracers and the signal of water stable isotopes ($\delta^{2}H$ and $\delta^{18}O$) smooth throughout the different compartments of the aquifer, with rapid variations in the unsaturated zone after recharge events and delayed effects in the saturated zone. At the same time, $\delta^{13}C_{TDIC}$ and nitrate values rise along the subsurface flow. While the carbon isotope evidences a shorter transit time between recharge areas and the top of the saturated zone than the subsequent path toward the permanent base springs, nitrate evolution is affected by pollution sources near discharge areas, so its applicability is questionable. Finally, organic matter (TOC and intrinsic fluorescence) mineralizes (or degrades) up to 90% from the first centimeters of soil to the permanent basal springs. An exponential decreasing trend defines the relationship between TOC and $\delta^{13}C_{TDIC}$ caused by organic matter attenuation along the groundwater flow path, while $\delta^{13}C_{TDIC}$ increases because of a higher residence time of water in contact with the host rock. These results, together with previous research based on other natural tracers (chemical, isotopes, and dating tools) and dye tracing experiences, permit to link TOC and $\delta^{13}C_{TDIC}$ values with a range of transit times, from hours-days to years-decades. Meanwhile, the attenuation of natural intrinsic fluorescence and TOC signal evidence the filter function of the aquifer from the soil to the saturated zone. All these findings highlight the usefulness of natural fluorescence and, particularly, TOC and $\delta^{13}C_{TDIC}$, as tracers of groundwater flow and hydrogeochemical processes within the different compartments of complex karst aquifers.

1. Introduction

Karst aquifers are one of the primary potable water sources worldwide since they provide 9.2% of the world's drinking water and contribute to 13% of the total global withdrawal of groundwater (Stevanović, 2019). These aquifers are formed by the dissolution of soluble rocks, such as limestone and dolostone, giving rise to a significant increment of intrinsic heterogeneity. This determines hydraulic properties, flow conditions, water–rock interactions, and hydrogeochemical processes occurring in karst aquifers (White, 1988). Rapid water infiltration through well-developed exokarstic landforms commonly represents a significant part of the aquifer recharge. However, it also takes place diffusely through carbonate outcrops, often covered by variable soil thickness. Therefore, the water-soil-rock

* Corresponding author.
E-mail address: delatorrem@uma.es (B. de la Torre).

https://doi.org/10.1016/j.jhydrol.2023.129392
Received 11 November 2022; Received in revised form 23 February 2023; Accepted 8 March 2023
Available online 13 March 2023

interaction and the bedrock architecture control the hydrogeology of the karst aquifers.

The hierarchized network of karst conduits allows a fast recharge transit and makes it possible at different time scales (Batiot, 2002; Serène et al., 2022). In this sense, the soil plays a key but complex role in the transformation of precipitation to groundwater (Wang et al., 2019) since it regulates hydrological processes such as evapotranspiration, runoff, infiltration, and hence the input of solutes within aquifers (Di Prima et al., 2020). In addition, CO_2 and organic acids in the soil drive the chemical dissolution of carbonate rocks (Yang et al., 2012), controlling the hydrochemical characteristics of the input signal together with the initial quality of rainwater and the degree of development of exokarst features. Commonly, the spatial distribution of soil and the permeable underlying bedrock is more heterogeneous in karst aquifers than in detrital systems. Therefore, a better insight into the processes that water undergoes in the soil-epikarst-unsaturated zone will help to better understand recharge processes, vulnerability to pollution episodes, and, in general, the hydrogeological functioning of carbonate aquifers.

Numerous studies have addressed hydrochemical and isotopic approaches to gain deeper insight into processes in different vertically distributed compartments of the aquifer. Some authors (e.g. Gazis and Feng, 2004; Sprenger et al., 2016; Chen et al., 2017) identified some isotopic processes undergoing soil water as soon as it infiltrates by sampling the liquid fraction at different depths. Wang et al. (2019) compared the hydrochemical and isotopic variations of water observed at different depths in various soil types. Lastennet (1994), Emblanch et al. (2003), Pronk et al. (2009), Lange et al. (2010), Azzaz et al. (2018), among others, investigated infiltration processes in carbonate aquifers from hydrochemical changes recorded in waters from the unsaturated zone. Savoy (2007) studied the natural attenuation of Total Organic Carbon -TOC- content in a karst aquifer. Serène et al. (2022), based on the method proposed by Ohno (2002), characterized rapid infiltration and quantified the transit time of conduit fluxes in the aquifer using TOC and intrinsic fluorescence related to natural organic matter as natural tracers. Other authors such as Barbel-Périneau et al. (2019) and Wang et al. (2020) carried out research on the hydrochemical and isotopic variations of temporary (overflow springs) and perennial springs. As the first ones drain the unsaturated zone and the latter relates more to the saturated zone, this monitoring strategy permits to infer the hydrogeological behavior of the system. Celle-Jeanton et al. (2003) deduced the participation of the saturated and unsaturated zone in a French Jura karst aquifer from the combination of chemical (NO_3^-, Mg^{2+} and TOC) and isotopic ($\delta^{13}C_{TDIC}$) parameters. Emblanch et al. (2003) used $\delta^{13}C_{TDIC}$ as an isotopic tracer to quantify the role of the unsaturated zone in different hydrodynamic states of the Vaucluse Karst systems. This has been subsequently evidenced in research such as Stuart et al. (2010), in a Maltese island, or Bicalho et al. (2019), in the Lez spring (France).

Despite these advances, few works jointly consider changes in the hydrochemical and isotopic signature of water along flowpaths from the soil-epikarst to the permanent springs. Lee and Krothe (2001) sought to identify changes in the infiltration signal from rainwater, soil, epikarst, and the saturated zone and to create a four-component mixing model to infer isotopic and hydrochemical fluxes in a karst aquifer in Indiana (USA). It is essential to know the variations in the infiltration signal through the soil-epikarst, unsaturated zone, and saturated zone of the aquifer to understand the transport and possible attenuation of contaminants. So, it is necessary to acquire a significant number of samples in the different vertical compartments of the aquifer (from the soil to the saturated zone) since their analysis helps to better understand the processes that transform the input signal (rainfall/infiltration) to groundwater; even more so in environments with complex geology.

The aims of this research are (1) to gain deeper insight into the hydrogeochemical processes occurring at the different compartments (soil-epikart-unsaturated/saturated zone) in geologically complex karst aquifers, from infiltration at the aquifer's surface to groundwater drainage by springs; and (2) discussing the complementarity of some specific natural tracers (TOC, intrinsic fluorescence related to organic matter, nitrates, $\delta^{13}C_{TDIC}$) as tools to reach a better understanding of groundwater flow dynamics semiquantitatively. As a pilot site, a tectonically complex karst aquifer, the Jarastepar carbonate massif, located approximately 65 km W of the city of Malaga in Southern Spain, has been selected (Fig. 1). Here, access to intermediate points of the groundwater flowpath is possible. Therefore, current study try to contribute with new data to the general previous knowledge on the processes occurring in the vertically distributed compartments of karst systems.

2. Setting

The Jarastepar massif extends over 56 km^2 in the western part of the Malaga province, in southern Spain (Fig. 1). The relief presents a steep orography, with altitudes ranging from 400 to 1400 m. This area has a typical Mediterranean climate, with a marked seasonal pattern in the annual precipitation variations and air temperature values. Rainfall and, therefore, recharge occur mainly from autumn to springtime. Climate conditions are also characterized by a dry season (usually up to 3–4 months), practically without rain, in summer. The mean annual precipitation recorded in this area during the period 1950/1951 to 2016/2017 was around 1050 mm (De la Torre et al., 2020), with a spatial distribution influenced by the barrier effect generated by the reliefs that constitute the study area, as well as those located immediately to the W against the humid winds coming from the SW. Thus, precipitation decreases from S to N: it was up to 1000 mm/y in the lower parts (southern border) and below 800 mm/y on the northern edge. The mean air temperature value for the available historical series (1997/1998 to 2016/2017) was 15.5 °C. The research period considered in this work (2015/2017) could be classified as slightly dry and warm, with an average precipitation of 934 mm/y and a mean air temperature of 15.8 °C.

Geologically, the Jarastepar massif is placed within the westernmost sector of the Betic Cordillera (Martín-Algarra, 1987; Balanyá et al., 2007) and presents a complex geological structure because of a large-scale tectonic contact. In this area, there are rocks from the three main tectonic domains of the Betic Cordillera (Fig. 1). At North, the External Zone (EZ) occupies the lowest tectonic position, constituted by 500–550 m of Jurassic limestones and dolostones, bounded by Triassic clays and evaporite rocks at the bottom, and Cretaceous-Paleogene marly-limestone at the top. At the South, the Internal Zone (IZ) overlaps the External Zone and consists of 1200 m of Triassic carbonate formations (Nieves Unit) and up to 400 m of Paleozoic metapelites (Alpujárride and Maláguide Complexes). Lastly, Tertiary brownish clays and sandstones belonging to the Flysch Complex are discontinuously imbricated between previous domains (defining the tectonic suture).

The three tectonic units overlap each other, with a general vergence toward the NW (Fig. 1). The set of geological units is affected by more recent strike-slip faults (NW-SE) and normal fractures (NE-SW and N-S). Background information about the geological and tectonic settings of the study area can be found in previous works (De la Torre et al., 2020; Gil-Márquez et al., 2020).

In hydrogeological terms, the dominant permeable formations are fractured and karstified Triassic and Jurassic carbonate rocks belonging to the Internal and External zones. Low-permeability materials limit these rocks at all their boundaries: Triassic clays, Cretaceous-Tertiary marls, and Paleozoic metapelites (Fig. 1). Dissolution processes have given rise to many exokarst features (karrenfields, dolines, sinkholes, among others) in Jurassic limestones of the External Zone, favoring recharge by infiltration of rainwater over the permeable outcrops. Previous works (Barberá et al., 2018; De la Torre et al., 2020; Gil-Márquez et al., 2020) revealed the hydrogeological behavior of the aquifer, from which a preliminary conceptual model was developed.

Most of the discharge occurs naturally through three permanent

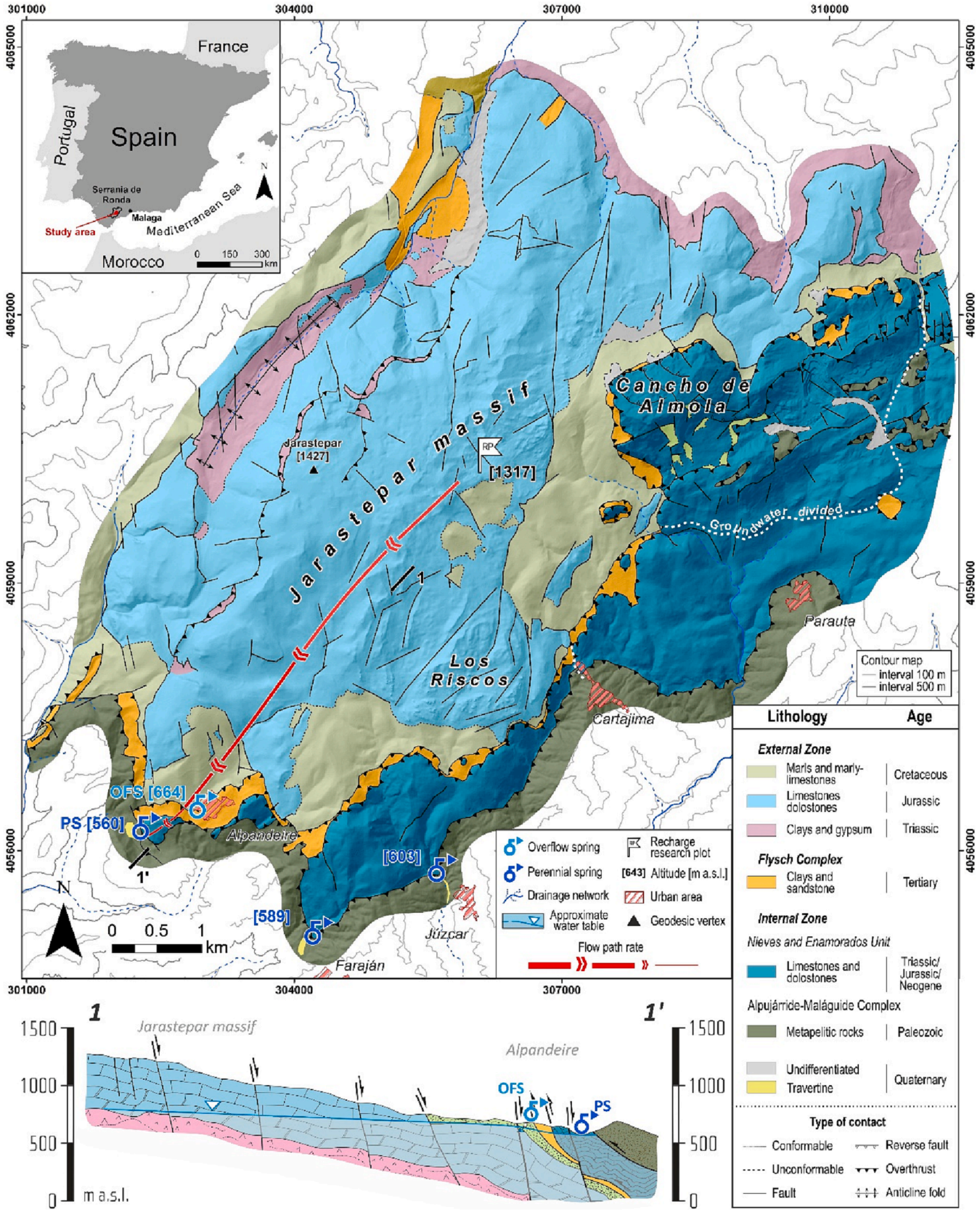

Fig. 1. Geographic location, geological sketch, and cross-section (1–1′) (modified from Gil-Márquez et al., 2020) representative of the study area. *OFS*, overflow spring; *PS*, perennial spring. Spring dataset in Table 1.

springs (PS) located at lower altitudes in the Triassic dolostones of the Internal Zone (Fig. 1): Huertos (560 m a.s.l.; mean discharge 25 l/s), Charco (589 m a.s.l; 23 l/s), and La Zúa (603 m a.s.l.; 204 l/s). In addition, two overflow springs (OFS) or ephemeral outlets (Alfaguara, 658 m a.s.l. and Pozancón, 664 m a.s.l.) are placed at the southern edge of the External Zone, just north of the major tectonic contact between the Internal Zone and the External Zone. The water table is accessible at the Pozancón overflow point in low water conditions through a 40 m deep vertical shaft. In any case, there are few cavities in the area, all with little development, so the characteristic of the unsaturated zone could not be directly observed for large distances. In the present study, the two overflow springs have been examined together due to their proximity and similar hydrogeological characteristics.

The most widely represented soil type in the study area (34%) is calcic leptosol, typical of mountainous reliefs, where the hardness of the rocks does not allow the development of soils thicker than 30 cm. Decalcification clays ("terra rossa") resulting from the gradual chemical weathering of carbonate rocks accumulate in karst depressions, such as dolines or uvalas, where the soil thickness is usually greater, reaching up to 75 cm. To a lesser extent (12%), calcareous regosols and solonchank exist, being soils somewhat more evolved than the previous ones, quite stony, and with strengths of around 50 cm. They usually appear on dolomitic rocks, favored by the presence of woody scrub or scattered holm oaks. According to the cartographic database of the Land Cover Information System of Spain (SIOSE, 2005, scale 1:25000), the recharge area is bare of vegetation or has rocky pastureland with scattered scrubland. Underneath this soil cover, the unsaturated zone has an estimated thickness between 400 and 600 m. Previous speleological explorations in the study area showed that there is some development of endokarstic morphologies, such as shafts or caves (De la Torre et al., 2020). These structures would favor the infiltration and flow of water throughout the aquifer.

3. Materials and methods

From February 2015 to March 2017, water samples were collected in different compartments distributed vertically into the aquifer to identify processes involved in the mineralization and degradation of organic matter along flowpaths, and to characterize the isotopic changes in water from infiltration towards the saturated zone. Soil water samples were collected from porous ceramic capsules installed at 30 and 60 cm depths (Fig. 2) in an experimental plot placed in the recharge area of the Jarastepar aquifer, at 1317 m a.s.l. (see location in Fig. 1). The soil type in karst depressions consists mainly of red decalcification clays. The experimental site also included an automatic weather station (DAVIS Vantage Pro2 model) for hourly rainfall and air temperature records and a rain collector with a filter funnel. A small volume of liquid paraffin was added to the latter to avoid evaporation of the rainwater sample.

Because of the accessibility to the water table, the Pozancón temporal spring (OFS in Fig. 1) was selected as the sampling point for fast groundwater flows in the aquifer. Meanwhile, Huertos spring (PS in this work) drains water from the saturated zone with longer residence time within the aquifer (De la Torre et al., 2020; Gil-Márquez et al., 2020). In both cases, water samples were collected at any hydrodynamic conditions during the control period.

16 rainwater and 31 soil water samples were collected in the experimental plot (Table 1): 15 samples at 30 cm deep and 16 at 60 cm. In addition, 138 water samples were taken from PS and 160 from the OFS. However, the discussion mainly focused on the water samples where all the parameters were analyzed. As a consequence of the free access to the water table in OFS, the samples collected can be classified according to the hydrodynamic state of the aquifer (De la Torre et al., 2020): piston flow (33 samples), outflowing (47), decline (35) and depletion (45). During the sampling periods, soil water could not be collected from every rainfall event, as a minimum volume of 41 ml was needed for the required analyses. Thus, soil water sampling was done for chemical and isotopic analyses during significant rainfall events. However, the soil water samples may represent accumulation from smaller rainfall events in other cases. It should be noted that water sampling at the different points make possible the hydrogeochemical comparison of data collected in the soil-epikarst and unsaturated zone with those from the saturated zone. In our case, the samples taken in the surface of the aquifer represent the infiltration signal (diffuse) into the system, while water from the springs brings together the different modes of recharge (diffuse and concentrated) hat feed the karst aquifer.

The ceramic composition of capsules can generate issues in the hydrochemical characterization of soil water samples. Adsorption, absorption, precipitation, and dilution frequently act during water flow through the porous material (Beier and Hansen, 1992; Sánchez-Pérez, 1994). For this reason, only the determination of total organic carbon (TOC), NO_3^- content, intrinsic fluorescence, and isotopic composition ($\delta^{18}O$, $\delta^{2}H$ y $\delta^{13}C_{TDIC}$) have been carried out in this work (Table 1). None of these parameters are affected by the physico-chemical processes previously mentioned (Weihermüller et al., 2007).

Chemical and isotopic analyses were performed in the Laboratory of the Centre of Hydrogeology at the University of Malaga (CEHIUMA). NO_3^- was determined using high-pressure ion chromatography (881 Compact IC Pro). The TOC concentration was measured with a SHIMADZU® V-TOC carbon analyzer. Natural fluorescence analysis of water samples was carried out in the laboratory using a PERKINELMER® brand spectrofluorimeter, model LS-55. $\delta^{18}O$ and $\delta^{2}H$ values of the water samples were measured using a compact isotope analyzer of the PICARRO® brand (Sunnyvale CA, USA), model CRDS L1102-i with autosampler, identical to that described by Gupta et al. (2009). For the analysis of $\delta^{13}C_{TDIC}$, a PICARRO® compact isotopic equipment, model G1111-i, was used, coupled to an Aurora 1030 TOC oxidation analyzer (Hartland et al., 2012).

The maximum intensity of each fluorescence peak is expressed in

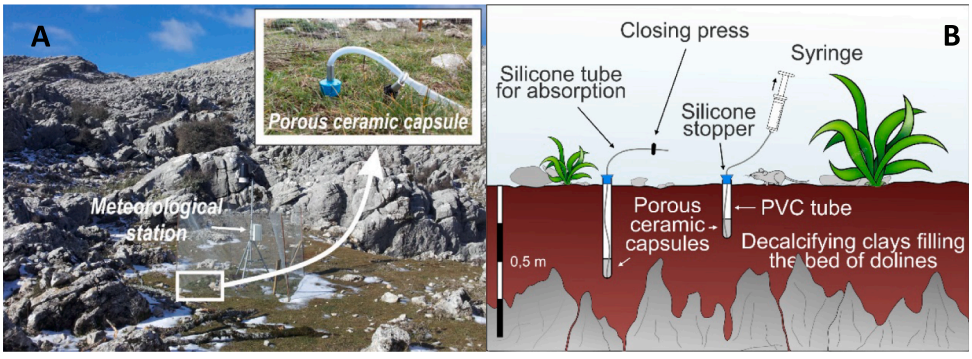

Fig. 2. (A) Experimental plot including porous ceramic capsules, the meteorological station, and the rain collector. (B) Schematic sketch with the porous ceramic capsules for water sampling in the soil at different depths (30 and 60 cm).

Table 1
Statistical parameters of the concentrations of NO_3^- and TOC; peaks A, C, T_1, T_2, and B of intrinsic fluorescence; and isotopic composition of $\delta^{18}O$, δ^2H, and $\delta^{13}C_{TDIC}$ analyzed from the water samples taken in this research, from February 2015 to March 2017. (n_t) number of total samples collected, (n_a) number of samples analyzed, (n_d) number of samples where each parameter has been detected, (min) minimum values, (max) maximum values, (σ) standard deviation, (cv) coefficient of variation, (nd) not detected. - Not analyzed or not calculated. *Bibliographic data (Clark and Fritz, 1997; Friedli et al., 1986; Cerling et al., 1991). [1], Statistical parameters of the groundwater samples in which the same parameters were measured as in the soil. [2], statistical parameters of the full set of groundwater samples collected during the study period.

Sampling point		NO_3^-	TOC	Natural fluorescence (RU)					$\delta^{18}O$	δ^2H	$\delta^{13}C$
		(mg/L)		A peak	C peak	T_1 peak	T_2 peak	B peak	‰ VSMOW		‰ VPDB
	n_d/n_a	16/16	–	–	–	–	–	–	15	15	–
Rainfall	*min*	0.7	–	–	–	–	–	–	−10.2	−64.7	–
1317	*max*	3.5	–	–	–	–	–	–	−3.6	−13.9	–
(m a.s.l.)	***median***	2.0	–	–	–	–	–	–	**−5.9**	**−32.7**	**−8.0***
$n_t = 16$	*σ*	0.8	–	–	–	–	–	–	1.9	14.5	–
	cv (%)	43	–	–	–	–	–	–	30	42	–
	n_d/n_a	15/15	15/15	15/15	15/15	15/15	15/15	14/15	11/11	11/11	11/11
Soil 30 cm	*min*	1.6	2.0	19.8	8.64	13.6	38.0	10.0	−9.2	−57.0	−21.5
1317	*max*	4.2	7.9	97.3	41.7	108.5	107.6	86.1	−4.0	−19.7	−15.1
(m a.s.l.)	***median***	**3.0**	**4.2**	**58.5**	**21.3**	**33.5**	**60.5**	**31.6**	**−5.8**	**−33.4**	**−18.0**
$n_t = 15$	*σ*	0.8	1.6	26.6	9.7	26.7	20.1	20.2	1.6	11.1	2.0
	cv (%)	25	36	46	43	59	31	63	24	28	11
	n_d/n_a	15/15	15/15	16/16	16/16	16/16	16/16	13/16	11/11	11/11	9/11
Soil 60 cm	*min*	1.7	0.6	15.4	4.07	10.5	19.5	11.2	−9.1	−58.1	−20.1
1317	*max*	5.2	4.6	74.1	27.5	170.5	159.8	44.8	−4.9	−24.8	−14.4
(m a.s.l.)	***median***	**3.9**	**1.6**	**36.7**	**12.8**	**31.9**	**58.8**	**26.9**	**−6.9**	**−40.7**	**−18.1**
$n_t = 16$	*σ*	0.92	1.2	16.1	6.6	41.4	40.1	12.3	1.4	11.3	2.1
	cv (%)	24	57	40	49	88	55	44	19	26	11
	n_d/n_a	17/17	16/16	17/17	17/17	0/17	2/17	0/17	16/16	16/16	17/16
Overflow spring[1]	*min*	2.9	0.5	3.2	1.4	nd	3.2	nd	−7.0	−41.5	−14.5
(OFS)	*max*	13.2	1.5	11.3	5.7	nd	5.6	nd	−5.5	−31.4	−8.2
643	***median***	**8.4**	**0.9**	**6.5**	**2.6**	**nd**	**4.4**	**nd**	**−6.2**	**−36.0**	**−12.0**
(m a.s.l.)	*σ*	2.6	0.3	2.7	1.4	nd	–	nd	0.4	2.9	1.8
$n_t = 17$	*cv (%)*	32	30	40	45	nd	–	nd	6	8	14
	n_d/n_a	17/17	16/16	16/16	13/16	0/16	0/16	0/16	16/16	16/16	17/17
Permanent spring[1]	*min*	3.8	0.2	0.1	0.1	nd	nd	nd	−6.9	−38.6	−6.9
(PS)	*max*	6.4	0.6	2.1	0.9	nd	nd	nd	−6.4	−37.1	−3.5
560	***median***	**4.7**	**0.3**	**0.8**	**0.4**	**nd**	**nd**	**nd**	**−6.6**	**−38.0**	**−5.8**
(m a.s.l.)	*σ*	0.7	0.1	0.5	0.3	nd	nd	nd	0.2	0.3	1.1
$n_t = 17$	*cv (%)*	14	32	60	60	nd	nd	nd	2	1	17
	n_d/n_a	160/160	160/160	17/17	17/17	0/17	2/17	0/17	81/81	81/81	135/135
Overflow spring[2]	*min*	1.2	0.3	3.2	1.4	nd	3.2	nd	−7.5	−43.7	−14.8
(OFS)	*max*	18.7	2.0	11.3	5.7	nd	5.6	nd	−5.6	−29.3	−8.2
643	***median***	**6.6**	**0.7**	**6.5**	**2.6**	**nd**	**4.4**	**nd**	**−6.4**	**−36.3**	**−12.8**
(m a.s.l.)	*σ*	3.2	0.3	2.7	1.4	nd	–	nd	0.4	3.1	1.0
$n_t = 160$	*cv (%)*	42	37	40	45	nd	–	nd	7	8	8
	n_d/n_a	138/138	138/138	16/16	13/16	0/16	0/16	0/16	86/86	86/86	137/137
Permanent spring[2]	*min*	2.1	0.1	0.1	0.1	nd	nd	nd	−7.1	−39.3	−8.9
(PS)	*max*	6.4	0.8	2.1	0.9	nd	nd	nd	−6.4	−37.0	−3.5
560	***median***	**4.3**	**0.3**	**0.8**	**0.4**	**nd**	**nd**	**nd**	**−6.6**	**−38.1**	**−5.8**
(m a.s.l.)	*σ*	0.8	0.1	0.5	0.3	nd	nd	nd	0.1	0.5	1.2
$n_t = 138$	*cv (%)*	17	39	60	60	nd	nd	nd	2	1	20

Raman units (RU), normalized according to the Raman peak intensity characteristic of the equipment. The isotopic values of $\delta^{18}O$ and δ^2H are referred to the Viena Standard Mean Ocean Water (VSMOW), while $\delta^{13}C_{TDIC}$ data correspond to the Viena Pee Dee Belemnite standard (VPDB).

4. Results

Table 1 shows the statistical parameters of the variables determined in soil, rain, and spring water samples taken in the framework of this research. The highest median contents of NO_3^- (8.4 mg/L) were recorded in OFS, while the lowest value (2.0 mg/L) was detected in rainwater. The NO_3^- concentration in soil water was slightly higher at 60 cm deep (3.9 mg/L) than at 30 cm (3.0 mg/L) (Table 1; Fig. 3A). In contrast, the highest TOC mean values (4.2 mg/L) were obtained at 30 cm deep, and it decreased as the infiltrated water flows vertically within the aquifer (Fig. 3B) until reaching the lowest mean concentrations in PS (0.3 mg/L). The coefficients of variation (*cv*) for the NO_3^- contents calculated for each sampling point were in the range of 14–43%; between 14% and 32% if rainwater samples are not considered. On the other hand, the TOC concentrations present a similar range, but between 30% and 57% (Table 1).

In general terms, the intensity of the intrinsic fluorescence was significantly higher in the soil water than in groundwater (Table 1). Peaks A and C, related to humic and fulvic acids, and peaks T_1 and T_2, linked to amino acids (Parlanti et al., 2000; Hudson et al., 2008), were recorded in all soil water samples, whereas tyrosine (peak B) was detected in most of them (Table 1). Only A and C fluorescence peaks were detected in groundwater, except twice T_2 peak in OFS. Waters taken at 30 cm deep showed a median fluorescence intensity for A and C peaks (58.5 and 21.3 RU) higher than at 60 cm (36.7 and 12.8 RU). The same pattern was observed for the fluorescence peaks corresponding to amino acids (T_1 and T_2) and B peaks (Table 1). The lowest median values of intrinsic fluorescence (A and C peaks) were recorded in the samples from PS.

Isotopic variability of the water molecule ($\delta^{18}O$ and δ^2H) reduces along the flowpath in the pilot site (Table 1; Fig. 3C). In rainwater samples, values are between −64.7 and −13.9‰, for δ^2H, and from −10.2 to −3.6‰ for $\delta^{18}O$. The median values of δ^2H detected in the soil water range between −33.4 y −40.7‰ for the samples collected at 30

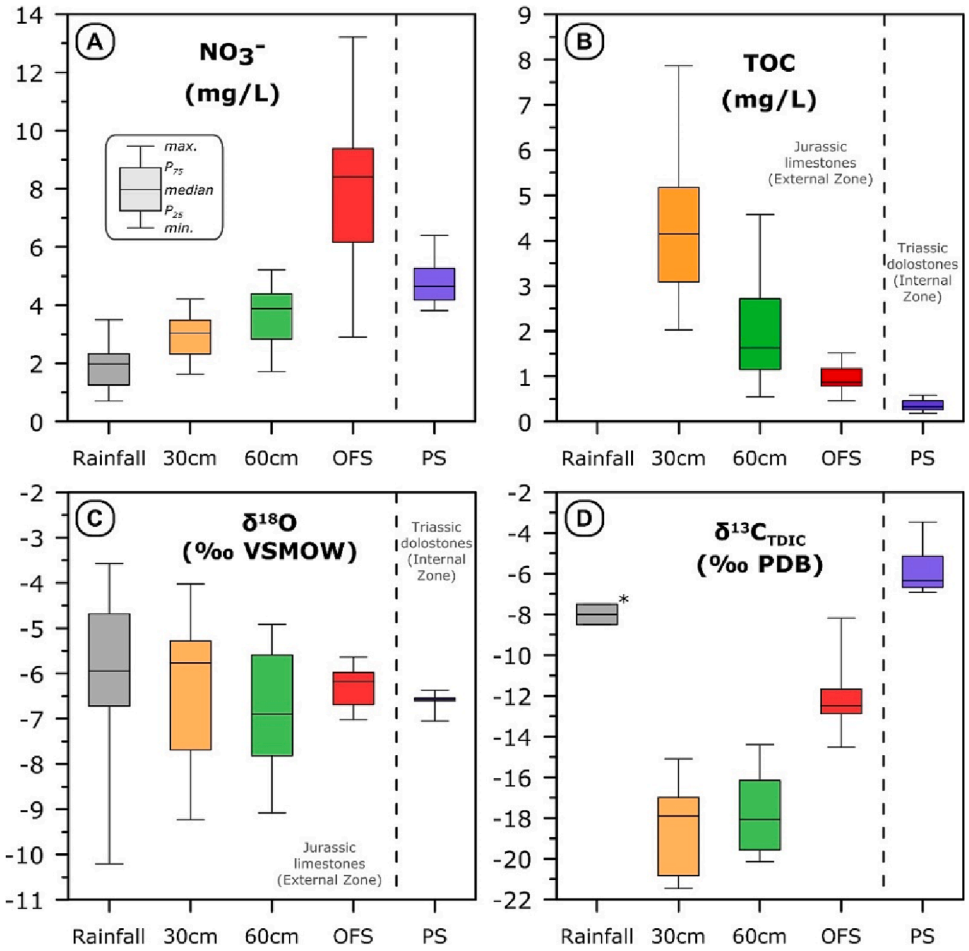

Fig. 3. Box and whisker plots of NO_3^- (A), TOC (B), $\delta^{18}O$ (C) and $\delta^{13}C_{TDIC}$ (D). Data from Table 1. At each box, points are ordered following the groundwater flowpath. *Value according to bibliography (Clark and Fritz, 1997; Friedli et al., 1986; Cerling et al., 1991).

and 60 cm depth, respectively; while the mean values of $\delta^{18}O$ range between −5.8 y −6.9‰ for the same control points. The median isotopic composition of groundwater is close to that of soil water since they vary between −36 y −38‰ for δ^2H, and between −6.2 and −6.6‰, for $\delta^{18}O$, in OFS and PS, respectively. Regarding the $\delta^{13}C_{TDIC}$ signal, median contents increased from the soil water samples (-18.1‰ at 60 cm deep) to the PS point (–5.8‰). Not enough volume of rainwater to analyze its $\delta^{13}C_{TDIC}$ signature was collected during the study period. A value in literature of −8.0‰ (Clark and Fritz, 1997; Friedli et al., 1986; Cerling et al., 1991) acts as a reference (Table 1; Fig. 3D).

On the other hand, the maximum value of fluorescence intensity of peak A and the TOC contents in water samples taken at the different control points show a positive correlation (Fig. 4). In general, values of the slopes representing the winter samples in the soil (m = 10.2) and the OFS (m = 8.1) are very similar. However, the slope resulting from the relationship above decreases along the flowpath, from the first centimeters of soil to the base-flow outlet (permanents springs) (Fig. 4). The intensity of fluorescence signal related to humic and fulvic acids along the flowpath in the aquifer decreases proportionally more than the organic matter content does. However, soil waters collected at 30 and 60 cm depth exhibit two straight lines with different slopes depending on the season: winter or spring (Fig. 4A and B). The steepest slopes correspond to the water samples collected in springtime. They show peak-A intensity versus TOC values higher than those in the winter months. In the OFS and the PS water samples, no different seasonal alignments have been detected as occurring in the soil.

Fig. 5 shows the temporal evolutions of TOC and NO_3^- contents, peaks A and C, and the $\delta^{13}C_{TDIC}$ measured in water samples from each control point. Records of discharge rate in PS and the variation of the water table registered in the vertical shaft of OFS are also plotted, as well as the daily rainfall measured in the pilot site during the study period. The sampled points presented markedly diverse hydrochemical (natural tracers) and isotopic ($\delta^{13}C_{TDIC}$) responses to precipitations events. In general, the soil and the OFS waters presented quick and sharp, as well as of more magnitude, variations in natural responses after rainfall. In contrast, groundwater drained by PS show lagged and buffered responses to precipitation events.

After the higher values of natural soil tracers (TOC, NO_3^-, and intrinsic fluorescence) recorded at the beginning of the hydrological year, a general progressive decreasing trend was observed in the soil and the overflow spring waters (OFS), interrupted by secondary peaks associated with recharge events occurring during the spring months (Fig. 5). In contrast, a different evolution pattern was observed in groundwater drained by the permanent spring (PS), characterized by two maximum values occurring at the beginning and the end of the year 2015/16, respectively.

The organic tracers decrease from the soil (30 cm) to the permanent spring waters. The lowering represents around two orders of magnitude for intrinsic fluorescence and one order of magnitude for TOC. In the soil waters, intrinsic fluorescence and TOC values are relatively similar but mostly lower at 60 cm deep. However, NO_3^- contents increase from rainwater to groundwater showing the highest values in the temporal spring (OFS).

The evolution of the $\delta^{13}C_{TDIC}$ values shows a trend towards less depleted values during the recharge periods, except in the PS water samples. In the first centimeters of the soil, the CO_2 produced by root

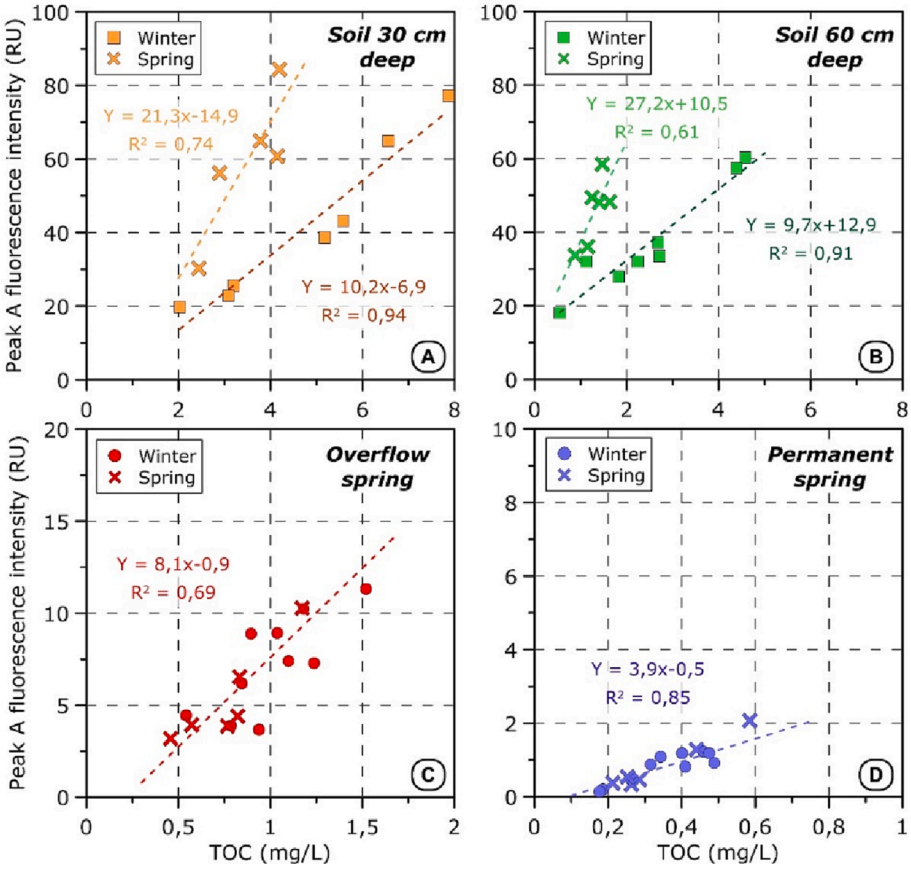

Fig. 4. Relationship between the maximum fluorescence intensity of peak A and TOC contents at (A) 30 cm depth in the soil, (B) 60 cm depth in the soil, (C) overflow spring (D), and the permanent spring. Data from Table 1. Note that the vertical axes of C and D are respectively 5 and 10 times smaller than in A and B, while the horizontal axes are 4 and 8 times smaller.

respiration (mostly C3 type plants) determines the $\delta^{13}C_{TDIC}$ signal in the water (~–22‰, Clark and Fritz, 1997; Drever, 1997; Deines, 1980). Rainwater infiltrated, with $\delta^{13}C_{TDIC}$ values in equilibrium with the atmosphere (~-8.0‰), acquires a more negative isotopic signal in the soil. The evolution of the $\delta^{13}C_{TDIC}$ values in the OFS waters is similar to that recorded for the soil water (Fig. 5), although with markedly less negative values. Finally, in the perennial spring (PS), the $\delta^{13}C_{TDIC}$ values show a general inverse trend to that of the soil water (Fig. 5).

As shown in Fig. 6, most of the analyzed water groups are located between the Eastern Mediterranean Meteoric Line (EMML) and the Global Meteoric Water Line (GMWL). The Local Meteoric Line (LML) shows values close to the Western Mediterranean Meteoric Line (WMML), although with a slightly smaller slope. The significant variability of rainwater samples progressively decreases from the soil (30 cm deep) to the permanent spring. The latter presents the most homogeneous values.

5. Discussion

The joint analysis of hydrochemical and isotopic results from the different sampling points evidences changes in groundwater throughout its transit within the vertically distributed compartments of the aquifer, from the soil and epikarst to the permanent outlet draining the saturated zone (Fig. 7). As direct infiltration of precipitation over the carbonate outcrops is the only groundwater input in the pilot site (De la Torre et al., 2020) the possibility that the variations recorded are due to the mixing of water from different sources is not considered, which is coherent with isotopic data (Fig. 6). Therefore, the changes recorded in the hydrochemical and isotopic signals must be a consequence of the characteristic of the meteoric water, the intrinsic characteristic of the system, the flow conditions within it, and the water-soil-rock interactions and related hydrogeochemical processes.

Intrinsic fluorescence, NO_3^- and TOC contents are widely used as infiltration tracers since they have an edaphic origin (Batiot et al. 2003a, b; Perrin et al., 2003; Mudarra et al., 2011; Serène et al., 2022). Denitrification processes do not seem to exist in the pilot site; this is consistent with oxidative conditions inside the aquifer (dissolved oxygen values in groundwater range between 3 mg/l -permanent spring- to 10 mg/l -overflow spring-). However, favorable conditions for this process in the deepest part of the system may be possible. On the other hand, it is not ruled out that small livestock farms and urban settlements may produce slight contamination, especially an enrichment of the NO_3^- contents. Generally, the highest concentrations of natural soil tracers were detected in groundwater at the beginning of the hydrogeological year due to soil leaching after months without rainfall (Fig. 5). Concentrations afterward decrease as recharge events occur during the rainy months (fall through spring). Nevertheless, there was occasional relative increases in NO_3^- and TOC concentration during some recharge events occurred in springtime (April 2016; Fig. 5). In soil waters, these rises of both parameters could be linked to the enhancement of biological activity occurring from March onwards due to increased air temperature (Fig. 5), while in the OFS the soil tracers peak are a consequence of the arrival of fast infiltration flows immediately recharge events. In the permanent spring, the highest tracer contents are recorded at the end of the recharge period, reflecting a delayed response to recharge events (De la Torre et al., 2020).

The NO_3^- concentration increases as rainwater infiltrates into the soil, doubling within the first 60 cm of soil (Fig. 4). According to literature (Peterson et al., 2002; Kalvāns et al., 2021), the increase of nitrate concentration in the soil is linked to leaching and/or evaporation

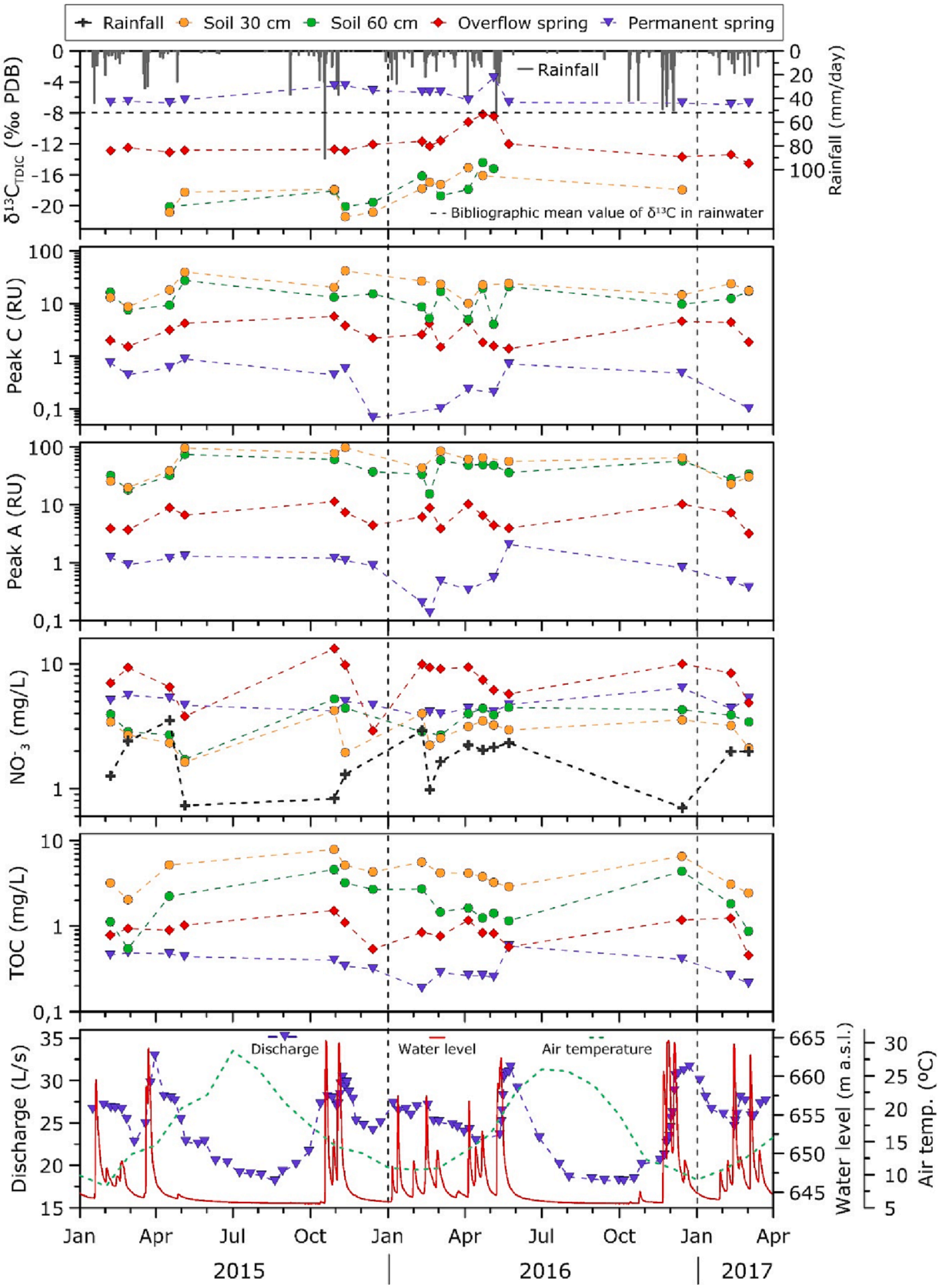

Fig. 5. Temporal evolution of the water level recorded in OFS, the discharge measured in PS, rainfall, air temperature, TOC and NO_3^- contents, intrinsic fluorescence (A and C peaks), and $\delta^{13}C_{TDIC}$ values determined at the different points selected in this study, from February 2015 to March 2017. Dataset from Table 1.

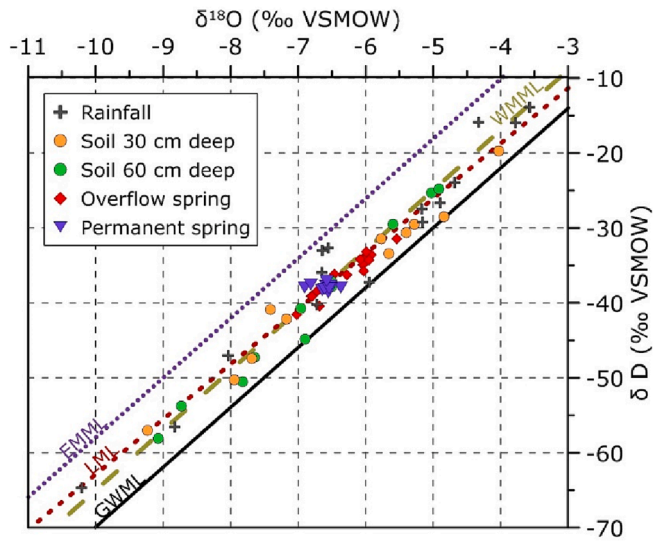

Fig. 6. Relationship between $\delta^{18}O$ and $\delta^{2}H$ values of meteoric water samples, soil water (capsules located at a depth of 30 and 60 cm), and groundwater (OFS and PS) in the samplings performed simultaneously at all points. The main meteoric lines are included: GMWL, Global Meteoric Water Line; LML, Local Meteoric Line; WMML, Western Mediterranean Meteoric Line; EMML, Eastern Mediterranean Meteoric Line.

processes. However, the isotopic values of soil water ($\delta^{18}O$ and $\delta^{2}H$; Fig. 6) do not reflect evidence of evaporation. At 30 cm depth, the soil has a higher effective porosity than at 60 cm due to a more significant biological activity, higher organic matter content, and therefore, less compaction (Franzluebbers, 2011). Thus, there is a more significant washout in the first 30 cm of soil, resulting in a higher accumulation of NO_3^- concentration at 60 cm, where there is less interstitial water flow because the soil is more compact and less porous (Chen et al., 2017). The OFS waters examined had higher NO_3^- concentrations (Table 1) in comparison with other near karst springs with similar land use in their recharge areas (Liñán, 2003; Barberá, 2014; Sánchez et al., 2017, De la Torre et al., 2020). This could be related to urban settlements and small family farms, leading to slight contamination from areas close to the temporal springs. However, this slight increase in NO_3^- values is attenuated as the groundwater fluxes circulate through the thick, saturated zone (Table 1; Fig. 3A) because of dilution associated with general homogenization of the infiltration signal (De la Torre et al., 2020).

Unlike carbonate aquifers located in humid regions with higher soil development and organic matter production (Batiot et al., 2003a; Pronk et al., 2006; Ravbar et al., 2012; Cholet, 2017), the concentration of TOC detected in groundwater was generally low; similar to those determined in nearby systems with similar climate characteristics (Barberá, 2014). Record of TOC contents throughout the aquifer shows a progressive decrease from values > 4 mg/L at the top -few centimeters of soil- to < 0.5 mg/L in the water drained by the permanent outlets (Table 1; Fig. 3B & 7). According to Batiot (2002), the mineralization of organic matter ($TOC \rightarrow HCO_3^-$) in carbonate aquifers (oxidizing environments) follows an exponential law as a function of time, with 70% of the organic carbon mineralization occurring after three months. Therefore, the TOC incorporated into the rainwater infiltrating the soil begins to mineralize in the first centimeters so that the average concentration recorded at 60 cm depth corresponds to half of that occurring at 30 cm. The mineralization of organic matter will continue through the unsaturated–saturated zone of the aquifer until it reaches minimum values in the saturated zone (Fig. 7).

Simultaneously, the coefficients of variation of TOC and $\delta^{18}O$ values decrease as water fluxes progress throughout the compartments of the aquifer, evidencing homogenization of the infiltration signal (Table 1; Figs. 3 & 7). This process is even appreciable in soil samples. The depth-dependent buffering of the infiltration signal in the soil-epikarst can be affected by factors such as mineralization of organic matter in the case of TOC content, or vegetation, soil porosity, rock fragment content, and topographic position, in the case of isotopic composition (Chen et al., 2017). The dispersion of the $\delta^{18}O$ and $\delta^{2}H$ values of the input signal (rainwater) is related to the characteristics of precipitation (seasonality, quantity, ambient temperature). Nevertheless, it does not present variations associated with the altitude effect (De la Torre et al., 2020), since

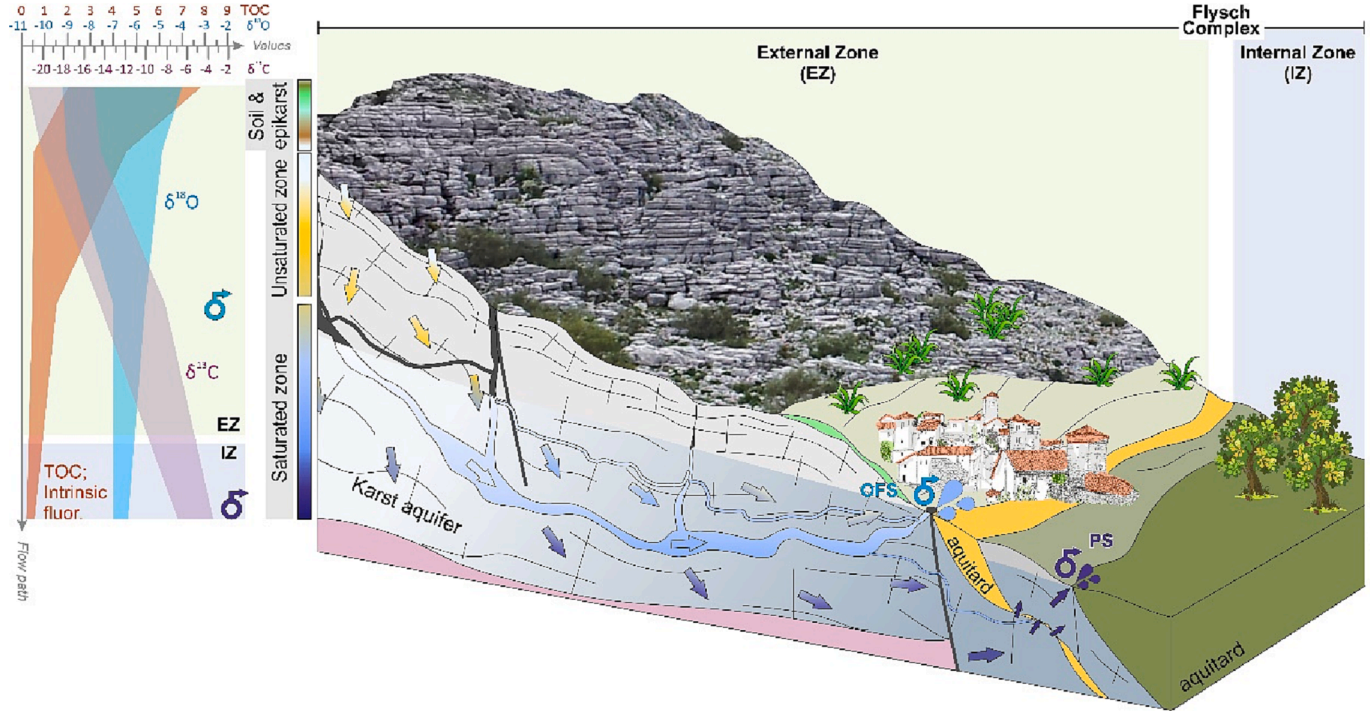

Fig. 7. Schematic illustration of the conceptual model developed in this research, with representation of the most relevant parameters vertically distributed.

most of the carbonate rocks forming the recharge area are found between 1000 and 1100 m a.s.l. In the current research, the variability of $\delta^{18}O$ is reduced by 20% in the first 30 cm of soil, while it diminished by 16% from 30 to 60 cm (Table 1; Figs. 3C & 7). Additionally, we found an attenuation rate of 70% in the unsaturated zone and 20% of the incoming $\delta^{18}O$ signal in the saturated zone. So, the total attenuation rate of the input signal in the flowpath was ~ 90%.

The homogenization of the input signal in the first centimeters of soil (30 cm) is mainly caused by the interception and absorption of water by plant roots (O'Driscoll et al., 2005). As the depth increased (>30 cm), where hardly any roots appear, the progressive decrease in soil porosity could be the cause. Consequently, due to a lower water renewal, a more significant NO_3^- accumulation at 60 cm depth occurs (Fig. 3A), consistent with the isotopic homogenization described above. In the saturated zone, the isotopic signature is near the mean weighted annual composition of precipitation (Clark and Fritz, 1997), which is observed in PS. Meanwhile, the fast-flow contribution to OFS produces greater variability around such value (Fig. 7).

On the other hand, the distinct seasonal variability in the TOC/peak A fluorescence intensity ratio in soil waters (Fig. 4) could be a consequence of the increased activity of the edaphic microbial community (bacteria, fungi, actinomycetes, among others) during the springtime, producing more humic and fulvic acids (Francioli et al., 2014; Barnard et al., 2015). The coefficient of variation of peak A decreases by 40% between 30 and 60 cm deep in the spring season. Similar to the highlighted parameters, the fluorescence intensity values become damped as rainwater leaves the soil and infiltrates through the unsaturated zone of the aquifer. In the waters drained by the OFS and the PS, the TOC/peak A relationships are the same for the winter and spring samples. This lack of seasonality corroborates that the waters infiltrating the aquifer underwent homogenization processes and signal damping beyond the first few centimetres of soil (Ford and Williams, 2007). Thus, intrinsic fluorescence is reduced by 90% in the unsaturated zone of the aquifer, and up to 98% until they are drained by the permanent springs located at a lower elevation.

The $\delta^{13}C_{TDIC}$ signature in groundwater is variable (Mook, 2000) depending on whether the system is open or closed (Clark and Fritz, 1997). The different sources of dissolved carbon in the water (CO_2 from the soil, organic matter, carbonate minerals, among others) have different isotopic compositions of carbon and contribute to the total dissolved carbon in different proportions. The openness of the carbonate aquifer to CO_2 entry controls the degree of dissolution of the rock matrix and the $\delta^{13}C_{TDIC}$ signature of groundwater (Clark and Fritz, 1997). In an open system, the C gas reservoir is considered infinite, and soil CO_2 is replenished during carbonate bedrock dissolution, resulting in lighter $\delta^{13}C_{TDIC}$ compared to a closed system (Clark and Fritz, 1997; Dreybrodt, 1998). Although most aquifers do not present purely open or closed system conditions (Fohlmeister et al., 2011), the behavior of the study area is more similar to an open system in the unsaturated zone, at least, as far as the Jurassic limestones are concerned. It should be noted that only 25% of the Externa Zone includes confining rocks, such us Cretaceous-Paleogene marly-limestone.

The temporal evolution pattern of $\delta^{13}C_{TDIC}$ values is alike in all sampling points, except for the permanent springs (Fig. 5). The progressive soil water renewal caused by successive precipitation events produces a bias towards less negative $\delta^{13}C_{TDIC}$ values (disequilibrium with the soil, –22‰, and more contribution of recently infiltrated water with signal closer to equilibrium with the atmosphere, −8‰). As already mentioned, soil biogenic CO_2 is directly influenced by the type of vegetation cover, which in Mediterranean enviroments corresponds mainly C3 type, with a $\delta^{13}C_{TDIC}$ signal of approximately of –22‰, while the isotopic signal of rainwater is −8‰. For it, after several months of no rainfall, the $\delta^{13}C_{TDIC}$ signal of CO_2 from plants (–22‰) dominates again in soil water. The $\delta^{13}C_{TDIC}$ signal of the samples collected in OFS is a mixing of soil (–22‰) and rainwater signal (–8‰), while the waters drained by the PS springs show a $\delta^{13}C_{TDIC}$ signal closer to equilibrium with the storage rock (0‰) (Fig. 3). This is due to fast flows between the recharge zone and the temporal drainage points (OFS), with transit times minimun of 15 h and flow velocities of up to 600 m/h into the unsaturated zone during recharge events, according to dye tracer test results (De la Torre et al., 2020). These flows are rapid and shallower in the aquifer, so the proportion of mixing and homogenization with stored water in the system would be low, which explains the distinct $\delta^{13}C_{TDIC}$ signal (Table 1; Figs. 3 and 7) and evolution pattern recorded in the PS (Fig. 5).

The general trend of $\delta^{13}C_{TDIC}$ in the soil water and in the OFS varies from lighter to heavier values throughout the hydrologic year (Fig. 5). This isotopic evolution is attributed to the progressive flushing that occurs in the soil of the recharge area. Thus, after the dry months, the soil water presents $\delta^{13}C_{TDIC}$ values close to the isotopic signal of the soil (~–22‰, -Clark and Fritz, 1997; Drever, 1997; Deines, 1980). However, following the recharge events generated during the autumn and winter, the $\delta^{13}C_{TDIC}$ detected in the OFS water evolve towards more negative values, reaching up to −14.5‰ (March 2017). In general terms, the waters of the permanent springs present an inverse trend throughout the hydrological year, from less negative values (around −4‰) to more depleted signatures (-7‰). This is consequence of the drainage of older water, with a higher equilibrium with the $\delta^{13}C_{TDIC}$ signal of the storage rock (0‰) during recession stages, which mix with more young water and with a $\delta^{13}C_{TDIC}$ signal far from equilibrium with the marine limestones after recharge events. In a previous study (Gil-Márquez et al., 2020), several groundwater dating techniques (^3H, ^3He, ^4He, and CFC–12) were applied together to explain the behavior of permanent springs of the study area. From the creation of lumped parameter models (binary mixing) and 5-bin shape-free models, two main flow components were identified. The mean age of the water drained by the permanent springs was found to be greater than decades (Table 2), with an old component that can be as old as 200 years. So, the average residence time of the waters drained by the PS located in the pilot site is considerably longer (about 100 years) than that of groundwater drained by the OFS (Fig. 8). Thus, the $\delta^{13}C_{TDIC}$ contents of the former are closer to equilibrium with the signal of the host rock (i.e., 0‰) and evolve slightly towards more negative values as recharge events occur during the hydrological year. The observed trend would be due to a rise in the proportion of the modern fraction reaching the outlet.

The joint use of TOC and $\delta^{13}C_{TDIC}$ (Figs. 7 & 8) shows the exponential decreasing trend associated with its attenuation along the groundwater flowpath, at the same time that $\delta^{13}C_{TDIC}$ increases because of the major residence time of water in contact with the host rock. The results obtained with both natural (chemical, isotopes, and dating tools) and dye tracers are in agreement with the transit times of hours-days deduced from results of dye tracers detected in OFS (De la Torre et al., 2020) and the age of years-decades inferred from dating results of PS (Gil-Márquez et al., 2020).

The different parameters related to the infiltration signal vary in different ways as the underground flow advances throughout the vertically distributed compartments of the aquifer (Figs. 7 and 8). Therefore,

Table 2
Results from groundwater distribution age models (Modified from Gil-Márquez et al., 2020. *Note: LW, IW and HW refer to low, intermediate and high water hydrodynamic situations, respectively. BMM, binary model mixing; DM, dispersion model; SFM, shape-free models. [a]Ages calculated assuming a $^4He_{rad}$ dissolution rate of $2{\cdot}10^{-7}$ ccSTP·kg/yr, according to the result of the lumped parameter model.*

Sampling point	System state	Tracer ages (years)			Mean age by BMM (DM-DM)	Mean age by 5-bin SFM
		$^3H/^3He$	$^4He^a$	CFC-12		
Permanent spring (PS)	*LW*	38	115		121	95
	IW	33	131			
	IW			42		
	HW	35	129			
	HW			43		

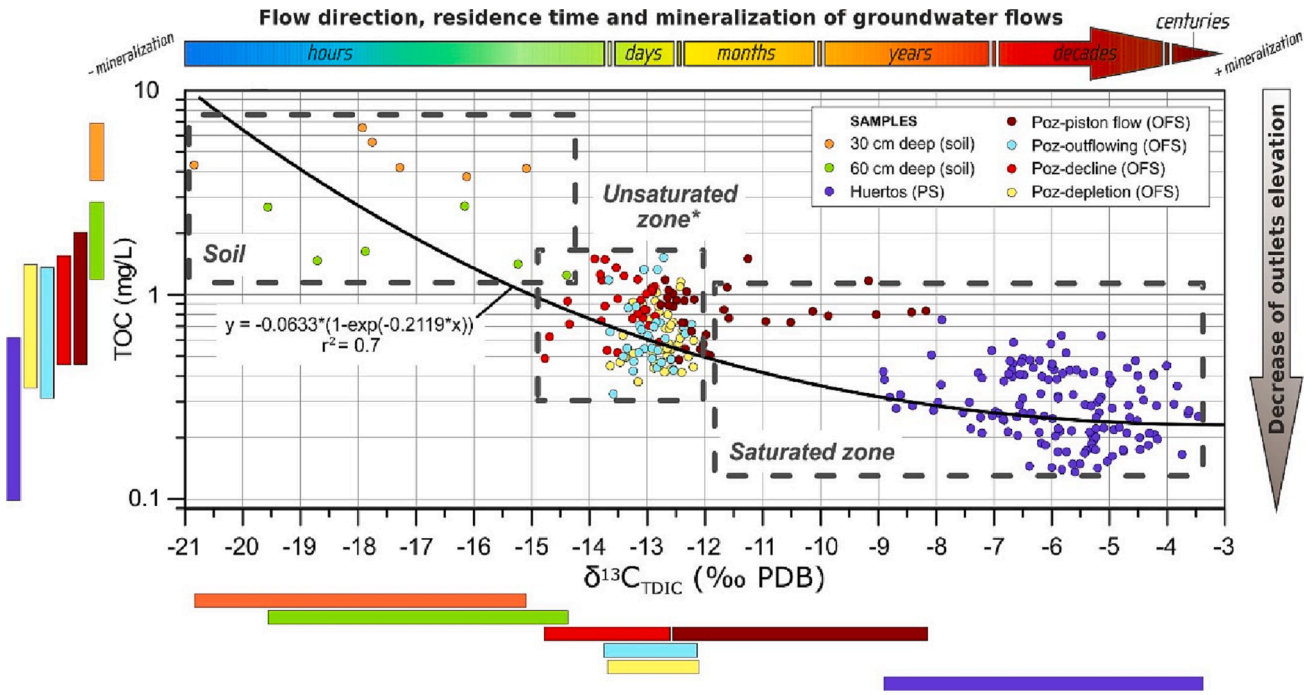

Fig. 8. Relationship between TOC (mg/L) and isotopic composition of $\delta^{13}C_{TDIC}$ (‰ PDB) of the total water samples collected at the different observation points of this research and representation of the ranges of values on the x and y axes. Water samples collected from Pozancón shaft (OFS) during different hydrodynamic conditions: *Poz-piston flow*, during the first hour after recharge; *Poz-outflowing*, when water table exceeds the overflowing threshold; *Poz-decline*, when aerial drainage stops but recharge water still arrives to the shaft; *Poz-depletion*, the lowest hydraulic head (dry season). **Unsaturated zone* includes the top of the saturated zone.

the joint combination provides information on infiltration and flow mechanisms and permits a qualitative estimation of the age of groundwater (Fig. 8). In this way, it follows that the same aquifer can quickly drain water with a residence time of hours (OFS), while moments before the same discharge point have been able to show water with several months or even a year within the system (piston flow). Lastly, there are waters with a residence time of up to hundreds of years drained by the permanent springs (Fig. 8). Therefore, all this shows that the flows in this type of media are not always fast. It should be noted that the proposed qualitative time scale in Fig. 8 presents uncertainties since the sampled groundwater is influenced by processes such as the mixture of flows of different origins (diffuse or concentrated infiltration, unsaturated zone, saturated zone) or the hydrodynamic conditions of the aquifer in the sampling time.

Therefore, in terms of natural tracers, it could be stated that the parameters related to intrinsic fluorescence and TOC are of greatest interest for the characterization of flows through unsaturated zone. Contrary to nitrate, both parameters are sensitive to seasonal variations in the soil, while nitrate concentration can be significantly affected by slight contamination in the system or denitrification processes. On the other hand, $\delta^{13}C_{TDIC}$ shows great interest in the aquifer as a whole since, from its values, it is possible to approximate the "relative age" of the flow through the different zones that constitute the aquifer. This can be reinforced if a joint analysis is carried out with the TOC, since the latter can be used as a fast flow tracer.

6. Conclusions

In this research, the joint application of hydrogeochemical and isotopic methods based on natural soil tracers (TOC, intrinsic fluorescence, NO_3^-, $\delta^{13}C_{TDIC}$) and water stable isotopes ($\delta^{18}O$, $\delta^{2}H$) deepened the understanding of recharge processes and groundwater flow dynamics through the different vertically distributed compartments in mountain karst aquifers. This way, it was possible to identify seasonal changes in the input signal and how such temporal variations are filtered and attenuated as the flow moves from the soil-epikarst towards the saturated zone. At the same time, this research has contributed to the knowledge of the hydrogeochemical processes involved in these changes (mineralization and degradation of organic matter along flowpaths). The results have shown the usefulness and complementarity of these techniques to improve the understanding of the hydrogeological functioning of karst aquifers, resulting in improved management of the water resources stored in them.

Seasonal variations in the concentration of natural soil tracers are transmitted and attenuated throughout the different compartments of the aquifer. Thus, such variations are detected rapidly (hours-days) in the unsaturated zone after recharge events, while they may take months to years to be registered in the saturated zone. In the first centimeters of the soil, leaching could be key to explaining the rise of nitrate with depth. As soil porosity decrease with depth, nitrate is more easily removed from the shallowest zone (30 cm), than with depth (60 cm). There are processes of mineralization (or degradation) of organic matter from the first centimeters of soil to the permanent springs, where TOC concentrations up to 90% lower than in the shallowest part of the system can be detected. Similarly, the mean values of intrinsic fluorescence, representing a small part of the total organic matter in the groundwater, are also reduced along the flow.

On the other hand, the spatial variations of the isotopic composition ($\delta^{18}O$) of groundwater have evidenced homogenization processes along the flow lines, as reflected by the progressive decrease in the coefficient of variation of this parameter (>90%). It should be noted that the $\delta^{18}O$ and $\delta^{2}H$ values have not evidenced evaporation processes in the soil. The gradual enrichment of the $\delta^{13}C_{TDIC}$ signal along the subsurface flow corroborates that the transit time between the recharge zone and the temporary spring is shorter than that until drainage by the permanent springs.

All these results combined have demonstrated the complementarity of natural tracers and the isotopic composition of groundwater for the identification of the processes taking place in the different vertical levels of the aquifer, especially within the unsaturated zone, as well as for the

semiquantitative temporal estimation of groundwater fluxes in these aquifers. Natural fluorescence and TOC are suitable parameters for recognizing the different processes mentioned than nitrates since slight anthropic contamination processes can significantly affect the latter's concentration. Likewise, $\delta^{13}C_{TDIC}$ is of great interest because, together with other parameters such as TOC, it makes it possible to qualitatively date subsurface flows in this type of systems.

As a final remark, highlight the need to advance in understanding the filter function and the physical and chemical processes that occur in the different compartment of karst aquifers. These are essential issues for developing reliable predictive models simulating future environmental conditions or anthropogenic changes.

7. Fundings

This research was supported by the project PID2019-111759RB-I00 funded by the Agencia Estatal de Investigación (AEI/https://doi.org/10.13039/501100011033) of the Spanish Government. Funding for open access charge: Universidad de Málaga / CBUA.

CRediT authorship contribution statement

B. de la Torre: Conceptualization, Methodology, Formal analysis, Investigation, Data curation, Writing – original draft, Writing – review & editing. **J.M. Gil-Márquez:** Conceptualization, Methodology, Formal analysis, Writing – review & editing. **M. Mudarra:** Conceptualization, Methodology, Investigation, Supervision, Funding acquisition, Project administration, Writing - review & editing. **B. Andreo:** Conceptualization, Formal analysis, Investigation, Resources, Writing – review & editing, Supervision, Project administration, Funding acquisition.

Declaration of Competing Interest

The authors declare that they have no known competing financial interests or personal relationships that could have appeared to influence the work reported in this paper.

Data availability

Data will be made available on request.

Acknowledgments

We thank to two anonymous reviewers who contributed to improving the original version of the manuscript, as well as to Corrado Corradini as Editor of Journal of Hydrology. This work is a contribution of the Research Group RNM-308 of the Junta de Andalucía.

References

Azzaz, H., Emblanch, C., Bekkoussa, B.S., Hamined, A., Khaldi, A., 2018. Impact of the unsaturated zone in the hydrochemical and hydrodynamical functioning of karst aquifer: example of the Tlemcen Mountains, Northwest Algeria. Arab. J. Geosci. 11, 454. https://doi.org/10.1007/s12517-018-3824-8.

Balanyá, J.C., Crespo-Blanc, A., Díaz Azpiroz, M., Expósito, I., Luján, M., 2007. Structural trend line pattern and strain partitioning around the Gibraltar Arc accretionary wedge: insights as to the mode of orogenic arc building. Tectonics 26 (2), n/a–n/a.

Barbel-Périneau, A., Barbiero, L., Danquigny, C., Emblanch, C., Mazzilli, N., Babic, M., Simler, R., Valles, V., 2019. Karst flow processes explored through analysis of long-term unsaturated-zone discharge hydrochemistry: a 10-year study in Rustrel, France. Hydrogeol. J. 27 (5), 1711–1723.

Barberá, J.A., 2014. Investigaciones hidrogeológicas en los acuíferos carbonáticos de la serranía oriental de ronda (Málaga). University of Malaga (Spain), p. 620. PhD Thesis.

Barberá, J.A., Mudarra, M., Andreo, B., De la Torre, B., 2018. Regional-scale analysis of karst underground flow deduced from tracing experiments: examples from carbonate aquifers in Malaga province, southern Spain. Hydrogeol. J. 26 (1), 23–40.

Barnard, R.L., Osborne, C.A., Firestone, M.K., 2015. Changing precipitation pattern alters soil microbial community response to wet-up under a Mediterranean-type climate. ISME J. 9 (4), 946–957.

Batiot, C., 2002. Étude expérimentale du cycle du carbone en regions karstiques. University of Avignon, (France), p. 254.. PhD Thesis.

Batiot, C., Emblanch, C., Blavoux, B., 2003a. Carbone organique total (COT) et Magnésium (Mg^{2+}): Deux traceurs complémentaires du temps de séjour dans laquifère karstique. C R Geoscience 335, 205–214. https://doi.org/10.1016/S1631-0713(03)00027-0.

Batiot, C., Liñán, C., Andreo, B., Emblanch, C., Carrasco, F., Blavoux, B., 2003b. Use of TOC as tracer of diffuse infiltration in a dolomitic karst system: the Nerja Cave (Andalusia, southern Spain). Geophys. Res. Lett. 30 (22), 2179. https://doi.org/10.1029/2003GL018546.

Beier, C., Hansen, K., 1992. Evaluation of porous cup soil-water samplers under controlled field conditions: comparison of ceramic and PTFE cups. J. Soil Sci. 43, 261–271. https://doi.org/10.1111/j.1365-2389.1992.tb00134.x.

Bicalho, C., Batiot, C., Taupin, J.D., Patriz, N., Van-Exter, S., Jourde, H., 2019. A conceptual model for groundwater circulation using isotopes and geochemical tracers coupled with hydrodynamics: A case study of the Lez karst system. France. Chem. Geol. 528, 118442 https://doi.org/10.1016/j.chemgeo.2017.08.014.

Celle-Jeanton, H., Emblanch, C., Mudry, J., Charmoille, A., 2003. Contribution of time tracers (Mg^{2+}, TOC, $\delta^{13}C_{TDIC}$, NO_3) to understand the role of the unsaturated zone: A case study—Karst aquifers in the Doubs valley, eastern France. Geophys. Res. Lett. 30 (6), 1322. https://doi.org/10.1029/2002GL016781.

Cerling, T.E., Solomon, D.K., Quade, J., Bowman, J.R. (1991). On the isotopic composition of carbon in soil carbon dioxide. Geochim. Cosmochim. Acta 55 (11): 3403-3405.

Chen, H., Hu, K., Nie, Y., Wang, K., 2017. Analysis of soil water movement inside a footslope and a depression in a karst catchment, Southwest China. Nat. Sci. J., Report 7, 2544. https://doi.org/10.1038/s41598-017-02619-x.

Cholet, C., 2017. Fonctionnement hydrogéologique et processus de transport dans les aquifères karstiques du Massif du Jura. University of Besançon, (France), p. 204. PhD Thesis.

Clark, I., Fritz, P., 1997. Environmental Isotopes in Hydrogeology. CRC Press LLC, p. 311.

De la Torre, B., Mudarra, M., Andreo, B., 2020. Investigating karst aquifers in tectonically complex alpine areas coupling geological and hydrogeological methods. J. Hydrol. X 6, 100047. https://doi.org/10.1016/j.hydroa.2019.100047.

Deines, P., 1980. The isotopic composition of reduced organic carbon. In: Fritz, P. y Fontes, J.C. (eds.), Handbook of Environmental Geochemistry, vol. 1, Amsterdam, Elsevier. 329-406.

Di Prima, S., Castellini, M., Rodrigo-Comino, J., Cerdá, A., 2020. Soil Hydrology for a Sustainable Land Management: Theory and Practice. Water J 12, 1109. https://doi.org/10.3390/w12041109.

Drever, J.I., 1997. The Geochemistry of Natural Waters: surface and groundwater environments. Prentice Hall, Upper Saddle River, New Jersey, p. 436.

Dreybrodt, W., 1998. Processes in Karst System. Springer. Berlin, Physics, Chemistry and Geology, p. 288.

Emblanch, C., Zuppi, G.M., Mudry, J., Blavoux, B., Batiot, C., 2003. Carbon 13 of TDIC to quantify the role of the unsaturated zone: the example of the Vaucluse karst systems (Southeastern France). J. Hydrol. 279, 262–274. https://doi.org/10.1016/S0022-1694(03)00180-X.

Fohlmeister, J., Scholz, D., Kromer, A., Mangini, A., 2011. Modelling carbon isotopes of carbonates in cave drip water. Geochim. Cosmochim. Acta 75 (18), 5219–5228. https://doi.org/10.1016/j.gca.2011.06.023.

Francioli, D., Ascher, J., Ceccherini, M.T., Pietramellara, G., 2014. Land use and seasonal effects on a Mediterranean soil bacterial community. J. Soil Sci. Plant Nutr. 4 (3) https://doi.org/10.4067/S0718-95162014005000057.

Franzluebbers, A.J., 2011. Stratification of soil porosity and organic matter. In: Jan Gliński, Józef Horabik and Jerzy Lipiec (eds.), Encyclopedia of Agrophysics. 10.1007/978-90-481-3585-1.

Friedli, H., Lötscher, H., Oeschger, H., Siegenthaler, U., Stauffer, B., 1986. Ice core record of the 13C/12C ratio of atmospheric CO_2 in the past two centuries. Nat. J. Sci. 324, 237–238.

Gazis, C., Feng, X., 2004. A stable isotope study of soil water: evidence for mixing and preferential flow paths. Geoder. 119, 97–111. https://doi.org/10.1016/S0016-7061(03)00243-X.

Gil-Márquez, J.M., De la Torre, B., Mudarra, M., Sültenfuß, J., Andreo, B., 2020. Complementary use of dating and hydrochemical tools to assess mixing processes involving centenarian groundwater in a geologically complex alpine karst aquifer. Hydrol. Process. 34 (20), 3981–3999.

Gupta, P., Noone, D., Galewsky, J., Sweeney, C., Vaughn, B.H., 2009. Demonstration of high precision continuous measurements of water vapor isotopologues in laboratory and remote field deployments using wave length scanned cavity ring down spectroscopy (WS CRDS) technology. Rapid Commun. Mass Spectrom. RCM 23, 2534–2542. https://doi.org/10.1002/rcm.4100.

Hartland, A., Baker, A., Timms, W., Shutova, Y., Yu, D., 2012. Measuring dissolved organic carbon $\delta^{13}C$ in freshwaters using total organic carbon cavity ring down spectroscopy (TOC CRDS). Environ. Chem. Lett. 10 (3), 309–315. https://doi.org/10.1007/s10311-012-0377-z.

Hudson, N., Baker, A., Ward, D., Reynolds, D.M., Brunsdon, C., Carliell-Marquet, C., Browning, S., 2008. Can fluorescence spectrometry be used as a surrogate for the Biochemical Oxygen Demand (BOD) test in water quality assessment? An example from South West England. Sci. Total Environ. 391, 149–158. https://doi.org/10.1016/j.scitotenv.2007.10.054.

Kalvāns, A., Popovs, K., Priede, A., Koit, O., Retiķe, I., Bikše, J., Dēliņa, A., Babre, A., 2021. Nitrate vulnerability of karst aquifers and associated groundwater-dependent ecosystems in the Baltic region. Environ. Earth Sci. 80, 628. https://doi.org/10.1007/s12665-021-09918-7.

Lange, J., Arbel, Y., Grodek, T., Greenbaum, N., 2010. Water percolation process studies in a Mediterranean karst area. Hydrol. Process. 24, 1866–1879. https://doi.org/10.1002/hyp.7624.

Lastennet, R., 1994. Rôle de la zone non-saturée dans le fonctionnement des aquifères karstiques. Approche par l'étude physico-chimique et isotopique du signal d'entrée et des exutoires du massif du Ventoux (Vaucluse). University of Avignon (France), p. 239.. PhD Thesis.

Lee, E.S., Krothe, N.C., 2001. A four-component mixing model for water in a karst terrain in south-central Indiana, USA. Using solute concentration and stable isotopes as tracers. Chem. Geol. 179 (1-4), 129–143.

Liñán, C., 2003. Hidrogeología de acuíferos carbonatados de la Unidad Yunquera Nieves (Málaga). University of Granada (Spain), p. 317.. PhD Thesis.

Martín-Algarra, A., 1987. Evolución geológica alpina del contacto entre las Zonas Internas y las Externas de la Cordillera Bética. University of Granada (Spain), p. 1171.. PhD Thesis.

Mook, W.G., 2000. Environmental isotopes in the hydrological cycle. Principles and applications. IHP-V. Technical Documents in Hydrology. N° 39, vol. IV. UNESCO, Paris. p. 196.

Mudarra, M., Andreo, B., Baker, A., 2011. Characterization of dissolved organic matter in karst spring waters using intrinsic fluorescence: Relationship with infiltration processes. Sci Total Environ 409 (18). https://doi.org/10.1016/j.scitotenv.2011.05.026.

O'Driscoll, M.A., DeWalle, D.R., McGuire, K.J., Gburek, W.J., 2005. Seasonal ^{18}O variations and groundwater recharge for three landscape types in central Pennsylvania, USA. J. Hydrol. 303, 108–124. https://doi.org/10.1016/j.jhydrol.2004.08.020.

Ohno, T., 2002. Fluorescence Inner-Filtering Correction for Determining the Humification Index of Dissolved Organic Matter. Environ. Sci. Tech. 36, 742–746. https://doi.org/10.1021/es0155276.

Parlanti, E., Wörz, K., Geoffroy, L., Lamotte, M., 2000. Dissolved organic matter fluorescence spectroscopy as a tool to estimate biological activity in a coastal zone submitted to anthropogenic inputs. Org. Geochem. 31, 1765–1781. https://doi.org/10.1016/S0146-6380(00)00124-8.

Perrin, J., Jeannin, P.Y., Zwahlen, F., 2003. Implications of the spatial variability of infiltration water chemistry for the investigation of a karst aquifer: a field study at Milandre test site. Swiss Jura. Hydro. J. 11 (673), 686. https://doi.org/10.1007/s10040-003-0281-5.

Peterson, E.W., Davis, R.K., Brahana, J.V., Orndorff, H.A., 2002. Movement of nitrate through regolith covered karst terrane, northwest Arkansas. J. Hydrol. 256, 35–47. https://doi.org/10.1016/S0022-1694(01)00525-X.

Pronk, M., Goldscheider, N., Zopfi, J., 2006. Dynamics and interaction of organic carbon, turbidity and bacteria in a karst aquifer system. Hydrogeol. J. 14 (4), 473–484. https://doi.org/10.1007/s10040-005-0454-5.

Pronk, M., Goldscheider, N., Zopfi, J., Zwahlen, F., 2009. Percolation and particle transport in the unsaturated zone of a karst aquifer. Ground Water 47 (3), 361–369. https://doi.org/10.1111/j.1745-6584.2008.00509.x.

Ravbar, N., Barberá, J.A., Petric, M., Kogovsek, J., Andreo, B., 2012. The study of hydrodynamic behavior of a complex karst system under low flow conditions using natural and artificial tracers (springs of the Unica River, SW Slovenia). Environ. Earth Sci. 65, 2259–2272. https://doi.org/10.1007/s12665-012-1523-4.

Sánchez, D., Barberá, J.A., Mudarra, M., Andreo, B., Martín, J.F., 2017. Hydrochemical and isotopic characterization of carbonate aquifers under natural flow conditions, Sierra Grazalema Natural Park, southern Spain. Geol. Soc. Lond. Spec. Publ. 466 (1), 275–293. https://doi.org/10.1144/SP466.1.

Sánchez-Pérez, J.M., 1994. Precauciones en el uso de los tomamuestras de succión equipados con porcelana porosa. Jornadas sobre investigación en medio no saturado. Ed. Ignacio Morell Evangelista. Castellón. Vol. 1. ISBN 84-8021-047-8. p. 164.

Savoy, L., 2007. Use of natural and artificial reactive tracers to investigate the transfer of solutes in karst systems. University of Neuchâtel, (France), p. 194.. PhD Thesis.

Serène, L., Batiot, C., Mazzilli, N., Emblanch, C., Babic, M., Dupont, J., Simler, R., Blanc, M., Massonnat, G., 2022. in karst hydrosystems. Application to the karst springs of Fontaine de Vaucluse system (Southeastern France). Hydrol. Earth Syst. Sci 26, 5035–5049. https://doi.org/10.5194/hess-26-5035-2022.

SIOSE (Sistema de Información sobre Ocupación del Suelo de España), 2005. Consejería de Medio Ambiente. Junta de Andalucía. Mapa de usos y coberturas vegetales del suelo de Andalucía. Base cartográfica SIOSE Andalucía a nivel de detalle, provincial de Málaga. 1:10.000. Consejería de Medio Ambiente. Junta de Andalucía.

Sprenger, M., Leistert, H., Gimbel, K., Weiler, M., 2016. Illuminating hydrological processes at the soil-vegetation-atmosphere interface with water stable isotopes. Rev. Geophys. 54, 674–704. https://doi.org/10.1002/2015RG000515.

Stevanović, Z., 2019. Karst waters in potable water supply: a global scale overview. Environ. Earth Sci. 78, 662. https://doi.org/10.1007/s12665-019-8670-9.

Stuart, M.E., Maurice, L., Heaton, T.H.E., Sapiano, M., Micallef-Sultana, M., Gooddy, D. C., Chilton, P.J., 2010. Groundwater residence time and movement in the Maltese islands– A geochemical approach. Appl. Geochem. 25, 609–620. https://doi.org/10.1016/j.apgeochem.2009.12.010.

Wang, F., Chen, H., Lian, J., Fu, Z., Nie, Y., 2020. Seasonal recharge of spring and stream waters in a karst catchment revealed by isotopic and hydrochemical analyses. J. Hydrol. 591, 125595 https://doi.org/10.1016/j.jhydrol.2020.125595.

Wang, Y., Shen, L., Chen, X., Wang, Z., Liang, X., Hu, B., Lan, J., Zhai, X., 2019. Response of soil water hydrochemistry and $\delta^{13}C_{DIC}$ to changes in spatio-temporal variations under different land covers in SW China karst catchment. Hydrol. Res. 50 (3), 925–944. https://doi.org/10.2166/nh.2019.061.

Weihermüller, L., Siemens, J., Deurer, M., Knoblauch, S., Rupp, H., Göttlein, A., Pütz, T., 2007. In Situ Soil Water Extraction: A Review. J. Environ. Qual. 36, 1735–1748.

White, W.B., 1988. Geomorphology and hydrology of karst terrains. Oxford Univ. Press, Nueva York (EEUU), p. 464.

Yang, L., Song, X., Zhang, Y., Han, D., Zhang, B., Long, D., 2012. Characterizing interactions between surface water and groundwater in the Jialu River basin using major ion chemistry and stable isotopes. Hydrol. Earth Syst. Sci. 16, 4265–4277.